JCTC Journal of Chemical Theory and Computation

Article

pubs.acs.org/JCTC

Diffusive Models of Membrane Permeation with Explicit Orientational Freedom

Jeffrey Comer,[†] Klaus Schulten,[‡,§] and Christophe Chipot*[,†,§]

[†]Laboratoire International Associé Centre National de la Recherche Scientifique et University of Illinois at Urbana−Champaign, Unité Mixte de Recherche No. 7565, Université de Lorraine, B.P. 70239, 54506 Vandoeuvre-lès-Nancy cedex, France

[‡]Department of Physics, University of Illinois at Urbana−Champaign, 1110 West Green Street, Urbana, Illinois 61801, United States

[§]Theoretical and Computational Biophysics Group, Beckman Institute for Advanced Science and Engineering, University of Illinois at Urbana−Champaign, 405 North Mathews, Urbana, Illinois 61801, United States

Supporting Information

ABSTRACT: Accurate calculation of permeabilities from first-principles has been a long-standing challenge for computer simulations, notably in the context of drug discovery, as a route to predict the propensity of small, organic molecules to spontaneously translocate biological membranes. Of equal importance is the understanding of the permeation process and the pathway followed by the permeant from the aqueous medium to the interior of the lipid bilayer, and back out again. A convenient framework for the computation of permeabilities is provided by the solubility−diffusion model, which requires knowledge of the underlying free-energy and diffusivity landscapes. Here, we develop a formalism that includes an explicit description of the orientational motion of the solute as it diffuses across the membrane. Toward this end, we have generalized a recently proposed method that reconciles thermodynamics and kinetics in importance-sampling simulations by means of a Bayesian-inference scheme to reverse-solve the underlying Smoluchowski equation. Performance of the proposed formalism is examined in the model cases of a water and an ethanol molecule crossing a fully hydrated lipid bilayer. Our analysis reveals a conspicuous dependence of the free-energy and rotational diffusivity on the orientation of ethanol when it lies within the headgroup region of the bilayer. Specifically, orientations for which the hydroxyl group lies among the polar lipid head groups, while the ethyl group recedes toward the hydrophobic interior are associated with free-energy minima $\sim 2k_BT$ deep, as well as significantly slower orientational kinetics compared to the bulk solution or the core of the bilayer. The conspicuous orientational anisotropy of ethanol at the aqueous interface is suggestive of a complete rotation of the permeant as it crosses the hydrophobic interior of the membrane.

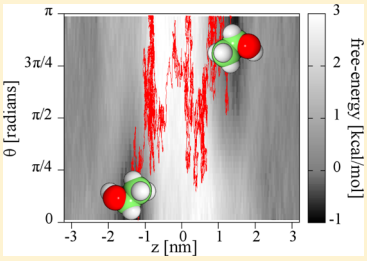

INTRODUCTION

Passive permeability of lipid bilayer membranes has conventionally been studied through the solubility−diffusion model,[1] from which the permeability can be related to the free-energy and diffusivity profiles along the normal to the bilayer. This model has been essential in the development at the experimental level of artificial membranes for rapidly screening lead compounds of pharmaceutical relevance on the basis of their membrane permeation potential,[2−6] as well as assisting the design of computational approaches to calculate permeabilities from first principles.[7−17] From the perspective of computer simulations, permeation can be viewed as a series of rare events. For this reason, computational approaches aimed at determining permeabilities invariably make use of importance-sampling strategies to calculate efficiently the underlying free energy.[18] While free-energy calculations have come of age and rest on the solid ground formed by the laws of statistical mechanics,[19] determination of kinetic parameters from simulations, like the diffusivity, has proven incrementally more challenging, because of the approximate nature of diffusive models.[20] Recently, probabilistic techniques, such as maximum-likelihood estimation and Bayesian inference, have been employed to determine the best kinetic parameters describing passive permeation.[13,17]

Computational approaches considering permeation as a one-dimensional diffusive process along the normal to the lipid bilayer have matured and are now able to yield permeabilities with at least semiquantitative agreement with experiment for simple molecules.[17] However, as recently underlined by Parisi et al.,[21] the influence of rare transitions along other degrees of freedom may come into play. In fact, the contribution of these degrees of freedom was shown to be appreciable, significantly impacting the rate constants associated with the translocation of solutes across the membrane. Recent work has taken into consideration the orientation of the permeant,[21] its protonation state,[16] deformation of the membrane,[22] and the coordination of the permeant by water, lipids, and other components of the molecular assembly.[13] For many permeants, orientational

Special Issue: Free Energy Calculations: Three Decades of Adventure in Chemistry and Biophysics

Received: March 12, 2014

   dx.doi.org/10.1021/ct500209j | J. Chem. Theory Comput. XXXX, XXX, XXX−XXX

diffusion, on the one hand, and the formation and extinction of water "fingers" extending into the bilayer,[11,23] on the other hand, occur on time scales comparable to that of translation along the normal to the bilayer, precluding one-dimensional calculation of the permeability.[21] Moreover, as noted by Hamming,[24] "the purpose of computing is insight, not numbers"—thus, while calculating bilayer permeabilities from first-principles is a laudable goal, of greater importance is the insight that can be gained from a coherent description of the transition pathway and how the latter relates to the atomic-scale interactions of the permeant, the lipids and water. In the context of transition pathways, the importance of degrees freedom coupled to the translational transition coordinate has been noted previously, notably in the case of the permeation of proteinaceous membrane channels by small alcohols.[25] These degrees of freedom, the movement of which spans time scales comparable to that of permeation, can be interpreted as hidden barriers of the free-energy landscape, hampering translational diffusion.

The inclusion of other degrees of freedom to the problem at hand adds wrinkles into the reconstruction of the free-energy and diffusivity hyperplanes, which, to the best of our knowledge, have not been addressed in a clear and general way. Here, we aspire to close the gap by developing a Bayesian-inference method to determine simultaneously free-energy and diffusivity landscapes along multiple coordinates. After outlining the theoretical background of the method, we apply it to unravel the contribution of both translational and orientational degrees of freedom in the permeation through a lipid bilayer of two prototypical solutes, namely, water and ethanol.

THEORETICAL UNDERPINNINGS

In a previous work,[17] we constructed diffusive models of water transport across a lipid bilayer, considering only displacements along the normal to the bilayer, which, in the present contribution, will be the z-axis of Cartesian space, defined relative to the center of mass of the bilayer. The Bayesian inference scheme[20,26,27] developed therein was applied to determine the free-energy and diffusivity one-dimensional (1D) profiles along this axis, i.e., $w(z)$ and $D(z)$, that best agreed with the simulation trajectories. Because of the high free-energy barrier for water to permeate a lipid bilayer (on the order of $10k_BT$), this scheme could not have been successful without the application of an importance-sampling method to guarantee uniform exploration of the transition coordinate. Our simulations incorporated time-dependent biasing forces,[28,29] which the Bayesian inference scheme is designed to handle.[27] It is worth noting that related solutions to the problem of determining position-dependent diffusivities from simulations featuring time-dependent biases have been put forth by Micheletti et al.[30] and, recently, for multidimensional systems, by Ljubetič et al.[31]

In the present work, we seek to extend the approach of ref 17 to accommodate a second coordinate, namely, the relative orientation of the permeant. With this addition, we determine the free energy and diffusivity as a function of both the position, z, relative to the bilayer, as well as the angle between the orientation vector of the molecule and the direction normal to the bilayer, θ. Extending the method for constructing the diffusive model to multiple coordinates is straightforward. Indeed, an earlier incarnation of the method was applied to two-dimensional (2D) translations.[26] As shown below, choosing the orientation angle as the second coordinate, however, requires additional care in the implementation.

Bayesian Inference Scheme. We start with a basic outline of the method, the description of which can be found in greater detail in refs 17 and 27. First, we select relevant collective variables to model the transition of interest—a single variable or combination thereof. Motion along the transition coordinate is assumed to correspond to a particular diffusive model. Thus far, we have considered overdamped Langevin dynamics, which has the free-energy landscape and position-dependent diffusivities as free parameters. In practice, the free energy can be represented directly, as in refs 17 and 32, or through the negative of its gradient, the mean system force, such as that in the original formulation.[27] Although the two approaches should in principle yield equivalent results, we have found that in the original mean force formulation, the optimization described below converges more rapidly. We seek the parameter values $\mathbf{H}^*$ that correspond best to the observed trajectory, denoted here by $\mathbf{T}$. The trajectory may be derived from simulations, or, alternatively, from experiment.[26]

We divide the trajectory into discrete steps, indexed by α, and choose initial trial values for the parameters $\mathbf{H}_0$. Using the rules of the diffusive model, we compute for each step $p(\{\mathbf{X}_{\alpha+1},t_{\alpha+1}\}|\{\mathbf{X}_\alpha,t_\alpha\},\mathbf{f}^{\text{bias}}(t_\alpha),\mathbf{H}_0)$, the probability of arriving at transition-coordinate configuration $\mathbf{X}_{\alpha+1}$ at time $t_{\alpha+1}$, given that the system was in configuration $\mathbf{X}_\alpha$ at time t_α, and, moreover, given the model parameters $\mathbf{H}_0$, as well as the biasing forces $\mathbf{f}^{\text{bias}}(t_\alpha)$. The probability of the entire trajectory, given the model parameters,[20,27,30] is the product of the probabilities at each step:

$$P(\mathbf{T}|\mathbf{H}_0) = \prod_\alpha p(\{\mathbf{X}_{\alpha+1}, t_{\alpha+1}\}|\{\mathbf{X}_\alpha, t_\alpha\}, \mathbf{f}^{\text{bias}}(t_\alpha), \mathbf{H}_0) \tag{1}$$

To determine the best set of parameters, we actually need the probability of the parameters given the trajectory—not the probability of the trajectory, given the parameters. From Bayes' theorem,[33,34] we can infer the former from the latter through

$$P(\mathbf{H}_0|\mathbf{T}) \propto P(\mathbf{T}|\mathbf{H}_0)p_{\text{prior}}(\mathbf{H}_0) \tag{2}$$

The prior probability of the trial parameters, $p_{\text{prior}}(\mathbf{H}_0)$, allows known features of the correct model parameters to be incorporated, which, heretofore, included scale-invariance,[35] smoothness of the functions serving as model parameters,[17,20,27] and close agreement with the free-energy landscapes determined by another method.[27] Finding the optimal parameters then becomes a problem of finding the set of parameters $\mathbf{H}^*$ that maximizes posterior probability $P(\mathbf{H}^*|\mathbf{T})$, which has been done in this work, as well as in previous ones,[27] using a Monte Carlo procedure and the Metropolis-Hastings[36] criterion to generate a Markovian chain of states $\mathbf{H}_j$.

Probability of the Trajectories. We compute the probability of each observed trajectory step, p_α, assuming that the set of M collective variables forming the transition coordinate $\mathbf{x} = (x^1, x^2, ..., x^M)$ undergoes overdamped Langevin dynamics on the time scale considered. Therefore, trajectories of the transition coordinate should satisfy the Brownian dynamics equation of motion:[37,38]

$$\dot{x}_t^i = \beta \sum_j D_{ij}(\mathbf{x}_t)F_j(\mathbf{x}_t, t) + \sum_j \nabla_j D_{ij}(\mathbf{x}_t) + \zeta_i(t) \tag{3}$$

dx.doi.org/10.1021/ct500209j | J. Chem. Theory Comput. XXXX, XXX, XXX−XXX

where $\dot{x}_t^i$ is the time derivative of collective variable i evaluated at time t; $\beta = (k_B T)^{-1}$; $D_{ij}(\mathbf{x}_t)$ is the (i, j) component of the diffusivity tensor for the configuration of the collective variables at time t; $F_j(\mathbf{x}_t, t)$ is the force on collective variable j for the configuration at time t, including any time-dependent biasing forces; ∇_j is defined as $\partial/\partial x_j$; and $\zeta_i(t)$ is a random noise with $\langle \zeta_i(t)\zeta_j(t')\rangle = 2D_{ij}(\mathbf{x}_t)\delta(t' - t)$.

Here, we consider a transition coordinate formed by two collective variables: z, the displacement of the center of mass of the permeant relative to the center of mass of the bilayer along the direction normal to the latter; and θ, the orientation angle of the permeant relative to the normal to the bilayer. Assuming a lack of hydrodynamic coupling between the motion along z and θ, the translational diffusion tensor component, $D_{zz}(z, \theta)$, and the rotational diffusion tensor component, $D_{\theta\theta}(z, \theta)$, are handled independently,[21] as opposed to an explicit roto-translational diffusion tensor, yielding

$$\dot{x}_t^i = \beta D_{ii}(\mathbf{x}_t)F_i(\mathbf{x}_t, t) + \nabla_i D_{ii}(\mathbf{x}_t) + \zeta_i(t) \tag{4}$$

with $\langle \zeta_i(t)\zeta_j(t')\rangle = 2D_{ij}(\mathbf{x}_t)\delta(t' - t)\delta_{ij}$.

In practice, we apply a discretized form of eq 4 to the trajectory, choosing a discretization time Δt that is sufficiently short, so that the displacements do not yield large changes in D_{ii} and F_i. Because molecular dynamics trajectories, at their heart, obey Newtonian mechanics — or some modification thereof, Δt must also be sufficiently long that motion is diffusive rather than ballistic, and consecutive displacements, i.e., $x_t^i - x_{t-\Delta t}^i$ and $x_{t+\Delta t}^i - x_t^i$, are uncorrelated.[31] For the motion along z, the discretization is simply

$$\begin{aligned} Z_{k+1} = Z_k + \beta[f_z(Z_k, \Theta_k) + f_z^{\text{bias}}(t_k)]D_{zz}(Z_k, \Theta_k)\Delta t \\ + \nabla_z D_{zz}(Z_k, \Theta_k)\Delta t + g_k\sqrt{2D_{zz}(Z_k, \Theta_k)\Delta t} \end{aligned} \tag{5}$$

where Z_k and Θ_k are trajectory values of z and θ at time $t_k = k\Delta t$. $f_z(z, \theta) = -\nabla_z w(z, \theta)$ is the negative of the z-component of the gradient of the free energy as a function of z and θ. g_k is a random variable. Assuming that $f_z(z, \theta)$, $f_z^{\text{bias}}(t)$, and $D_{zz}(z, \theta)$ do not change substantially over Δt, g_k can be assumed to obey a standard normal distribution. With normally distributed g_k and given the trial functions $\mathbf{f}(z, \theta)$ and $D_{zz}(z, \theta)$, the probability density of a displacement $Z_{k+1} - Z_k$ is given by

$$P[Z(t)|f_z(z, \theta), D_{zz}(z, \theta)] \approx \prod_k \frac{1}{\sqrt{4\pi D_{zz}(Z_k, \Theta_k)\Delta t}} \exp\left(-\frac{\{Z_{k+1} - Z_k - \beta D_{zz}(Z_k, \Theta_k)[f_z^{\text{bias}}(t_k) + f_z(Z_k, \Theta_k)]\Delta t - \nabla_z D_{zz}(Z_k, \Theta_k)\Delta t\}^2}{4D_{zz}(Z_k, \Theta_k)\Delta t}\right) \tag{6}$$

However, diffusion in θ can be understood as a random walk on a sphere, having a measure of $\sin\theta\, d\theta$, which, in principle, does not yield Gaussian distributions, even in the case of zero force and constant uniform diffusivity. This nonuniform measure can be interpreted as adding an effective geometrical term $E_{\text{eff}}(\theta) = -k_B T \ln \sin\theta$ to the free-energy landscape. For initial positions Θ_k and time intervals Δt, where the probability of approaching the domain boundaries ($\theta = 0$ and π) remains close to zero, the Bayesian scheme is able to capture the slowly varying energy term E_{eff}. Indeed, applying the method used here to a permeant in bulk solution, where its orientation is isotropic, yields $w(z, \theta) \approx E_{\text{eff}}(\theta)$. Removal of geometric contributions[39] from plotted free energies can be misleading, as the resulting quantity does not mirror the actual probability distribution; thus, all free-energy plots in this work implicitly incorporate the $-k_B T \ln \sin\theta$ dependence. Near the domain boundaries, the measure becomes zero and the effective energy becomes infinite—a situation that cannot be handled by a discrete approximation such as that shown in eq 6. A sufficiently accurate and computationally efficient method to determine the distribution near the end points consists of using the solution of the diffusion equation with reflecting boundaries,[40] which corresponds to an infinite series of image Gaussians centered outside the domain of θ. Assuming that the typical displacement in time Δt is small, compared to the domain length, $\theta_b - \theta_a$, where $\theta_a = 0$ and $\theta_b = \pi$, the infinite series can be approximated by two image Gaussians. Defining the drift (μ_k) and variance (σ_k^2) as

$$\begin{aligned} \mu_k = \beta D_{\theta\theta}(Z_k, \Theta_k)[f_\theta^{\text{bias}}(t) + f_\theta(Z_k, \Theta_k)]\Delta t \\ + \nabla_\theta D_{\theta\theta}(Z_k, \Theta_k)\Delta t \end{aligned}$$

and

$$\sigma_k^2 = 2D_{\theta\theta}(Z_k, \Theta_k)\Delta t \tag{7}$$

we approximate the probability density by a Gaussian centered at the initial position plus the sum of two Gaussians centered beyond each of the domain end points:

$$\begin{aligned} P[\theta(t)|f_\theta(z, \theta), D_{\theta\theta}(z, \theta)] \approx \prod_k \frac{1}{\sqrt{2\pi\sigma_k^2}}\left\{\exp\left[-\frac{(\Theta_{k+1} - \Theta_k - \mu_k)^2}{2\sigma_k^2}\right] + \exp\left[-\frac{(\Theta_{k+1} + \Theta_k - 2\theta_a + \mu_k)^2}{2\sigma_k^2}\right]\right. \\ \left. + \exp\left[-\frac{(\Theta_{k+1} + \Theta_k - 2\theta_b + \mu_k)^2}{2\sigma_k^2}\right]\right\} \end{aligned} \tag{8}$$

To validate the use of eq 8, we performed a molecular dynamics simulation of a single ethanol molecule in pure water, where the molecule should have a uniform orientational diffusivity, because of the isotropy of the medium. Figure S1 in the Supporting Information shows that the Bayesian scheme augmented with eq 8 is able to yield an orientational diffusivity roughly uniform in θ for the isotropic case. On the other hand, assuming a Gaussian probability profile, as in eq 6, results in significant systematic error in the calculated diffusivity near the domain end points.

METHODOLOGICAL DETAILS

The calculations described in this work began with molecular dynamics simulations, in which an adaptive biasing force was applied to improve sampling along the 2D transition coordinate formed by a translational and rotational component. The

dx.doi.org/10.1021/ct500209j | J. Chem. Theory Comput. XXXX, XXX, XXX−XXX

trajectories were analyzed to determine the optimal values of the parameters of the diffusive model, using Monte Carlo sampling in parameter space and a Bayesian inference scheme to determine the likelihood of each set of parameters. Below, we describe these procedures in further detail.

Molecular Dynamics Simulations. The present work investigates the permeation of a water and an ethanol molecule through a membrane model. The two molecular assemblies consisted of a bilayer patch of 100 1-palmitoyl-2-oleoyl-*sn*-phosphatidylcholine (POPC) units solvated by 9294 water molecules, identical to that used in the work of Comer et al.,[17] barring, in the case of alcohol permeation, the addition of a single ethanol molecule. The simulated system had dimensions of approximately 5.9 nm × 5.9 nm × 11.6 nm, with periodic boundary conditions enforced along all three directions of Cartesian space. The lipid bilayer spanned the *xy* plane, making it effectively infinite in many respects.

The simulations were executed in the molecular dynamics software NAMD 2.9,[41] using the protocols described in Comer et al.[17] Based on the results of this paper, we chose the TIP3P water model, a 0.8−0.9 nm van der Waals cutoff, and the Lowe-Andersen thermostat. The latter thermostat was implemented using the default parameters of NAMD 2.9 to maintain the temperature at 308 K. A constant pressure of 101.325 kPa was maintained by means of the Langevin piston method.[42] Electrostatic interactions were computed via the particle-mesh Ewald algorithm,[43] with a mesh spacing of <0.12 nm and a short-range cutoff of 0.9 nm. Interactions involving atoms of POPC and ethanol were calculated according to the CHARMM36 Force Field[44] and the CHARMM General Force Field,[45] respectively. The NAMD option vdwForceSwitching was activated for a faithful reproduction of CHARMM36 lipid models. The equations of motion were integrated by the r-RESPA multiple timestepping scheme[46] with steps of 2 and 4 fs for short- and long-range interactions. The length of covalent bonds including hydrogen atoms were constrained[47,48] to the values prescribed by the CHARMM force field.

Importance-Sampling Strategy. The adaptive biasing force[28,29] method was utilized on the 2D space[39] of z and θ, with the implementation in the colvars module[49] of NAMD 2.9. In practice, z was defined by $[\mathbf{r}(\mathrm{X}) - \mathbf{r}(\mathrm{P, N})]\cdot\hat{z}$, where $\mathbf{r}(\mathrm{X})$ is the center of mass of water or ethanol, $\mathbf{r}(\mathrm{P, N})$ is the center of mass of all P and N atoms in the POPC bilayer, and $\hat{z}$ is a unit vector along the z axis of the simulated system. For water, the orientational angle θ was the angle between the z axis and the vector from the O atom to the center of mass of the H atoms, $[\mathbf{r}(\mathrm{H_2}) - \mathbf{r}(\mathrm{O})]\cdot\hat{z}$, while, for ethanol, θ was the angle between the z axis and the vector $\mathbf{r}(\mathrm{Et}) - \mathbf{r}(\mathrm{OH})$, where $\mathbf{r}(\mathrm{OH})$ and $\mathbf{r}(\mathrm{Et})$ are the center of mass of the hydroxyl and ethyl groups, respectively. As prescribed by the adaptive biasing force method, the 2D transition coordinate was discretized and force samples along z and θ were collected in bins, which had widths of 0.02 nm and 5°, respectively. To enhance sampling, the reaction pathway was stratified in five overlapping windows over intervals in z of [−32,0], [−24,8], [−16,16], [−8,24], [0,32], and [28,44]. Each window sampled the complete range of θ, namely, $[0,\pi]$.

Bayesian Reconstruction of Diffusive Models. Both the mean system force, $\mathbf{f}(z, \theta)$, and the diffusivities, $D_{zz}(z, \theta)$ and $D_{\theta\theta}(z, \theta)$ were discretized by means of cubic interpolants on a grid identical to that used in the importance-sampling simulations, namely, $z \in [-32,32]$ with a grid spacing of 0.02 nm, and $\theta \in [0,\pi]$ with a grid spacing of 5°. For $D_{zz}(z, \theta)$ and $D_{\theta\theta}(z, \theta)$, the values at the grid nodes were constrained to be greater than 0.1 nm^2/ns and 0.003 rad^2/ns, respectively, which is significantly smaller than any expected value. However, even when the values at the grid nodes are constrained to be positive, the cubic interpolants sometimes yield negative values, which are not permitted for diffusivity; thus, trial diffusivity functions where any negative diffusivity value appears in eq 6 or eq 8 were rejected. Displacements were observed on time intervals Δt = 2 ps, which previously[17] appeared in agreement with the results of the diffusive model and the direct measurement of the permeability. Scale-invariant priors were applied to $D_{zz}(z, \theta)$ and $D_{\theta\theta}(z, \theta)$, while smoothness priors were applied to all model parameters, $\mathbf{f}(z, \theta)$, $D_{zz}(z, \theta)$, and $D_{\theta\theta}(z, \theta)$,[27] using restraints of 50 kcal/(mol nm^2), 5 nm/ns, and 174 rads/ns.[17] The free-energy as a function of z and θ was determined by integrating F_z and F_θ, using the Monte Carlo scheme implemented in the program abf_integrate.[39]

Brownian Dynamics Simulations. The Brownian dynamics simulations were employed to explore the properties of the diffusive model consisting of $w(z, \theta)$, $D_{zz}(z, \theta)$, and $D_{\theta\theta}(z, \theta)$. The time step was chosen as $\Delta\tau$ = 20 fs to allow the dynamics to stabilize over the free-energy landscape. Consecutive steps of the simulation were generated according the following propagators:

$$z_{k+1} = z_k + \beta D_{zz}(z_k, \theta_k) f_z(z_k, \theta_k)\Delta\tau + \nabla D_{zz}(z_k, \theta_k)\Delta\tau + g_k^0\sqrt{2D_{zz}(z_k, \theta_k)\Delta\tau} \quad (9)$$

$$\theta_{k+1} = \theta_k + \beta D_{\theta\theta}(z_k, \theta_k) f_\theta(z_k, \theta_k)\Delta\tau + \nabla D_{\theta\theta}(z_k, \theta_k)\Delta\tau + g_k^1\sqrt{2D_{\theta\theta}(z_k, \theta_k)\Delta\tau} \quad (10)$$

where g_k^0 and g_k^1 are random numbers obeying a standard normal distribution. There is no need to include the geometric contribution in the latter equation, because it is assumed to be already included in $f_\theta(z, \theta) = -\partial_\theta w(z, \theta)$. The functions $\mathbf{f}(z, \theta)$, $D_{zz}(z, \theta)$, and $D_{\theta\theta}(z, \theta)$ were evaluated using cubic interpolation such as that during the Bayesian reconstruction.

RESULTS AND DISCUSSION

Below, we determine the dependence of the free energy and diffusivity of water and ethanol on their location and orientation, relative to the bilayer. We then leverage these free energies and diffusivities to construct a diffusive model of ethanol permeation and perform with the latter Brownian dynamics simulations to probe the properties of likely pathways.

Water. Extracting a water molecule from the polar environment of the bulk phase and bringing it to the center of a lipid bilayer is an energetically costly process—akin to the dehydration free energy of water.[50] Indeed, Marrink and Berendsen[7] calculated a barrier of 6.2 ± 0.5 kcal/mol at 350 K, using 1,2-dipalmitoyl-*sn*-phosphatidylcholine (DPPC) lipids, the Berger lipid force field,[51] and the SPC water model,[52] while Holland et al.[12] calculated a barrier of ∼5.4 and 5.8 kcal/mol at temperatures of 323 and 350 K, respectively, using the same lipid species, the CHARMM36 lipid force field,[44] and the TIP3P[53] water model. For POPC lipids at 308 K, we obtained[17] barriers of 6.7 ± 0.2 and 7.2 ± 0.2 kcal/mol with the TIP3P[53] and TIP4P-Ew[54] water models, respectively, also employing the CHARMM36 force field.[44] This free-energy barrier is primarily

dx.doi.org/10.1021/ct500209j | J. Chem. Theory Comput. XXXX, XXX, XXX−XXX

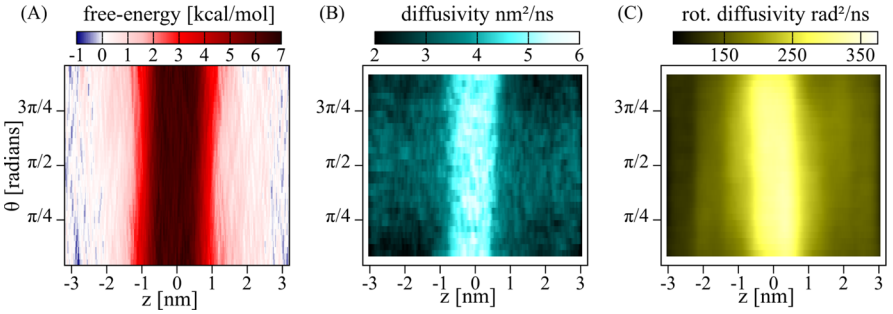

Figure 1. Diffusive model of water transport across a lipid bilayer: (A) free energy, as a function of the position relative to the plane of the bilayer (z) and the orientation of the water molecule (θ); (B) translational diffusivity $D_{zz}(z, \theta)$, as a function of z and θ; (C) rotational diffusivity $D_{\theta\theta}(z, \theta)$, as a function of z and θ. By convention, $z = 0$ corresponds to the center of the hydrophobic interior of the lipid bilayer.

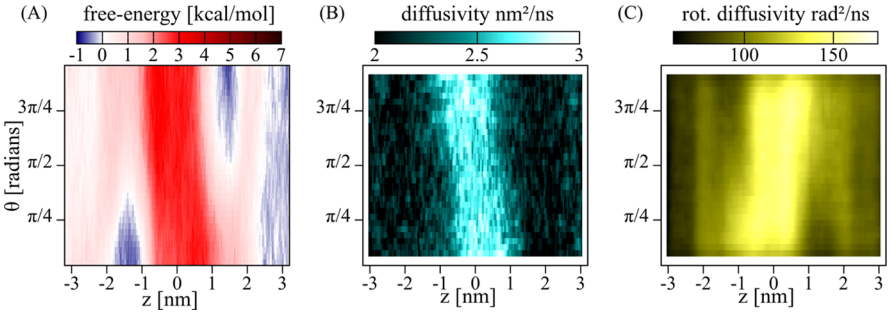

Figure 2. Diffusive model of ethanol transport across a lipid bilayer: (A) free energy, as a function of the position relative to the plane of the bilayer (z) and the orientation of the ethanol molecule (θ); (B) translational diffusivity $D_{zz}(z, \theta)$, as a function of z and θ; (C) rotational diffusivity $D_{\theta\theta}(z, \theta)$, as a function of z and θ.

responsible for the relatively low membrane permeability of water.

Here, we consider the free-energy landscape of water as a function of z and θ, shown in Figure 1A. We find a barrier along the z-axis with the height consistent with the value of 6.7 ± 0.2 kcal/mol measured from the corresponding one-dimensional free-energy profile,[17] using identical simulation parameters. This barrier spans the abscissa uniformly, with no significant variation along θ. Therefore, it would appear that there is little coupling between translational and orientational transitions for water, which, given the roughly spherical shape of the permeant, is not completely unexpected.

Figure 1B reveals the dependence of the diffusivity on z and θ. Along z, we find a maximum diffusivity of ∼6 nm^2/ns near the center of the bilayer and a minimum of ∼2 nm^2/ns near z = ± 1.5 Å, which is consistent with our previous results,[17] as well as those of Holland et al.,[12] determined by a different method. In the present work, we are now able to discern an appreciable θ-dependence, namely that the diffusivity minimum in the headgroup region of the bilayer seen in the 1D profile is absent when θ nears $\pi/2$.

Furthermore, the analysis in the present work yields the orientational diffusivity as a function of both the position and orientation, which is shown in Figure 1C. Like the translational diffusivity, the orientational diffusivity is larger within the lipid tails than elsewhere. One can infer from Figures 1B and 1C that the rotational relaxation is significantly faster than the translocation process—specifically, the water molecule is likely to completely reorient ∼10 times in the course of its translocation. Thus, rotational relaxation of water molecules is unlikely to be a rate-limiting process in their permeation through lipid bilayers.

It follows from the present findings that water may not be the best candidate to represent druglike compounds, because of its small size and the short orientational relaxation time. Ethanol, on the other hand, in addition to being an actual drug—albeit nowadays usually a recreational one, possesses a marginally bulky hydrocarbon group and a polar hydroxyl group. Thus, it is conceivable that, for ethanol, translocation and reorientation might be more intertwined, especially at the highly anisotropic water/membrane interface. Below, we elucidate a substantial orientation dependence in the free energy and diffusivity landscapes of ethanol.

Ethanol. The free energy, as a function of the position and orientation of ethanol, relative to the membrane, is shown in Figure 2A. In contrast to water, an orientation dependence is perceptible, most notably through the existence of two free-energy minima appearing in the headgroup region of the membrane near $\theta = 0$ and $\theta = \pi$. These minima are ∼2k_BT deep. As illustrated in Figure 3, these minima correspond to configurations in which ethanol lies at the boundary between the headgroup region of the membrane and the hydrophobic core, oriented such that the hydroxyl moiety remains near the head groups, while the ethyl group recedes into the tail region. Conversely, the opposite orientation (with the hydroxyl group pointing into the hydrophobic core of the bilayer) is associated with an extension of the free-energy barrier along z, resulting in an apparent S-shaped motif in Figure 2A. Indeed, the barrier spans from approximately −0.7 to 1.0 nm at $\theta = 0$, while at $\theta = \pi$, it ranges from about −1.0 nm to 0.7 nm. As may be expected from the less-polar nature of ethanol, compared to water, the free-energy barrier for translocation is ∼2 times less, i.e., 3 kcal/mol on average.

As shown in Figure 2B, the translational diffusivity along z shows a clear increase in the hydrophobic core of the bilayer,

dx.doi.org/10.1021/ct500209j | J. Chem. Theory Comput. XXXX, XXX, XXX−XXX

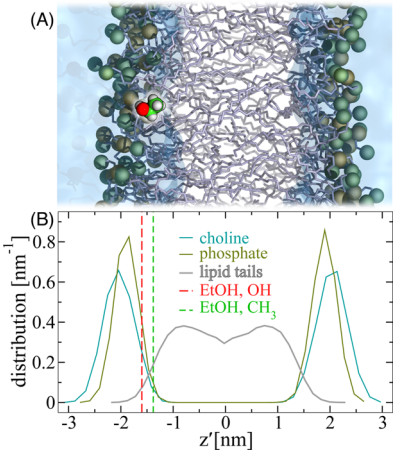

Figure 3. Detail of the relative positions of ethanol and chemical components of the membrane for values of z and θ corresponding to the free-energy minimum. (A) Snapshot of the trajectory showing a typical configuration of the system for values of z and θ, corresponding to the leftmost free-energy minimum in Figure 2A. The ethanol molecule is shown in a space-filling representation, with carbon, oxygen, and hydrogen atoms colored, respectively, green, red, and white. Choline and phosphate groups are displayed as turquoise and brown spheres, respectively, while the remaining parts of the lipid molecules are represented by blue-gray sticks. Water molecules are not shown explicitly, but indicated by a translucent blue surface. (B) Distribution of ethanol and lipid atoms in simulation frames for which $z \in [-1.8,-1.2]$ Å and $\theta < \pi/6$, i.e., near the leftmost free-energy minimum. The positions of the atoms along the normal to the bilayer, relative to its center of mass, are referred to z', because z has been reserved for the analogously defined position of the ethanol center of mass. The labels "choline" and "phosphate" correspond to the distribution of the choline N atom and phosphate P atoms of the POPC, while "lipid tails" refers to the distribution of the sn1 and sn2 C atoms of POPC. The coordinates of the hydroxyl and methyl groups of ethanol are shown as vertical lines, because the domains of z and θ that were considered restrict their observed positions near the mean values indicated by the lines, with standard deviations of ∼0.16 nm.

with respect to the value in the bulk aqueous medium, which is consistent with the rule of thumb that permeants involved in stronger interactions with their environment will diffuse slower than they would in an inhospitable milieu with weaker interactions. This z dependence is qualitatively similar to what we observed for water, although the diffusivity, generally, is significantly lower. Interestingly enough, the S-shaped pattern of the free-energy barrier to decreasing values of z as θ increases from 0 to π, is mirrored in $D_{zz}(z, \theta)$. It is worth noting that, at variance with the results of Ghaemi et al.,[13] we obtain a larger diffusivity for ethanol in the hydrophobic core of the membrane than in the bulk aqueous medium. This discrepancy may be ascribed to the use of differing force fields, as well as differences in the approach.

The orientational diffusivity of ethanol (see Figure 2C) also shows an appreciable θ-dependence. Specifically, there are minima in $D_{\theta\theta}(z, \theta)$ that appear when the ethanol lies between the headgroup and tail regions of the membrane and is aligned in the manner opposite to that corresponding to the minima of the free energy (c.f. Figure 2A), namely, with the hydroxyl moiety oriented toward the tail region. Just like for water, the orientational diffusivity of ethanol is greatest in the hydrophobic interior of the membrane.

Analysis of the Diffusive Model. Assuming the validity of the standard solubility−diffusion model,[1,21] we compute the permeability coefficient using

$$\frac{1}{P} = \int_{-L}^{L} \mathrm{d}z \frac{\exp(+\beta w(z))}{D(z)} \tag{11}$$

where $\pm L$ represent the boundaries of the bilayer. To obtain the 1D potential of mean force $w(z)$, we integrate the gradients obtained by the adaptive biasing force method.[32] The 1D diffusivity, $D_{zz}(z)$, was obtained by applying the Bayesian scheme in one dimension as in ref 17. While results for water are given in the latter reference, for ethanol, we obtain a permeability of 2.0 ± 0.2 cm/s.

This result is more than an order of magnitude larger than that calculated by Ghaemi et al.,[13] 0.085 ± 0.004 cm/s, which is a difference that can likely be attributed to their use of a longer displacement time scale (Δt) and a different force field, as the latter simulations employed the General Amber Force Field[55,56] for all components, rather than the CHARMM36[44] and CHARMM General Force Field,[45] used here for lipids and ethanol, respectively. The difference in temperature (323 K versus our 308 K) may also be significant. For hydrophilic permeants such as water and ethanol, the integral in eq 11 is dominated by the free-energy barrier in the hydrophobic core of the membrane, as well as the diffusivity there. While we obtain a barrier of 2.5 ± 0.2 kcal/mol, Ghaemi et al. obtained a value of 3.5 ± 0.2 kcal/mol, which is sufficient to make our

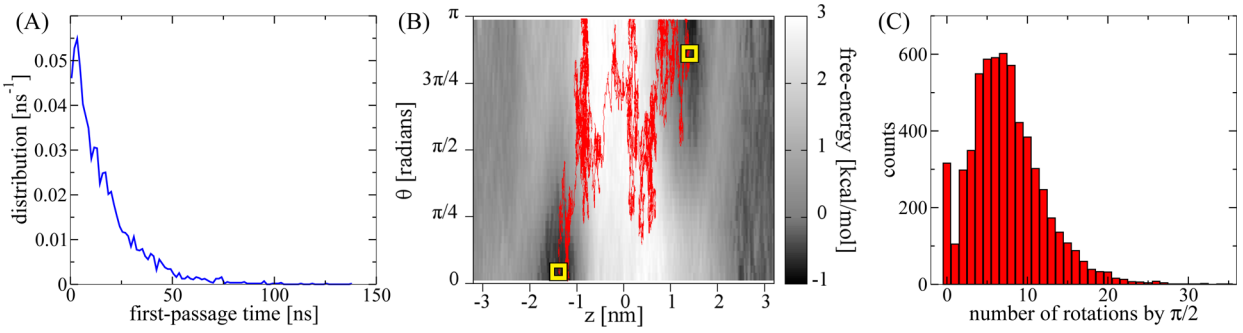

Figure 4. Results of Brownian dynamics simulations of ethanol permeation based on the diffusive model represented in Figure 2. (A) First passage-time distribution from the minimum at $z = -1.4$ nm and $\theta = \pi/36$ to $z = +1.4$ nm. (B) A typical permeation trajectory crossing from $z = -1.4$ to +1.4 nm. The particle representing ethanol enters from near the free-energy minimum on the side of the plot and near the free-energy minimum on the right-top. The trajectory is shown as a red curve faithfully overlaying the free-energy landscape, which is represented in grayscale. The initial and final positions are indicated by cyan squares. (C) Number of quarter-rotations of the ethanol particle during permeation over the above interval.

dx.doi.org/10.1021/ct500209j | J. Chem. Theory Comput. XXXX, XXX, XXX−XXX

value larger by a factor of 5. We calculate a diffusivity of ∼3.5 nm^2/ns in the hydrophobic core, which is similar to that calculated by Ghaemi et al. for an observation time of Δt = 15 ps. However, the authors use the diffusivity calculated over a longer observation time to calculate their final result, D = 0.95 nm^2/ns, which increases our permeability value by a factor of 3, relative to theirs.

The functions $w(z, \theta)$, $D_{zz}(z, \theta)$, and $D_{\theta\theta}(z, \theta)$ represented in Figure 2 comprise a complete diffusive model of the translational and rotational dynamics of the permeant in the vicinity of the bilayer. The diffusive model contains only two degrees of freedom, z and θ, as opposed to the molecular dynamics simulations described earlier in the text, which involve ∼41 000 particles, amounting to ∼88 000 positional degrees of freedom after subtracting the number of constrained bonds. Thus, the diffusive model represents a dramatic simplification of the system, dispensing with many details inherent in the molecular dynamics description while gaining conceptual clarity and the potential for vastly increased computational efficiency.

To explore the implications of the model, we ran 4000 Brownian dynamics simulations in which a particle representing ethanol was initially at the point z = −1.4 nm and $\theta = \pi/36$, near the free-energy minimum. The particle was constrained to z > −2.0 nm, and the simulations were terminated when the particle reached z = 1.4 nm, signifying that it had crossed the bilayer. Figure 4A shows the distribution of the time at which z = 1.4 nm was first attained.

An important question is whether reorientation of the permeant is fast enough to occur during the permeation process, or whether the permeant remains kinetically trapped in the orientation in which it began permeation.[21] For this purpose, we pruned a long, 400-μs Brownian dynamics trajectory into subsets that begin at one boundary point (z = −1.4 nm or +1.4 nm) and end at the other, without recrossing the first boundary between them. Figure 4B shows a typical permeation subtrajectory, which, like many such trajectories, begins near one of the two free-energy minima and ends near the other. During each permeation subtrajectory, we recorded the number of times that the orientation of the permeant underwent a cumulative change greater than $\pi/2$, which is shown in Figure 4C. Clearly, in most cases, ethanol is able rotate over large intervals several times; thus, we conclude that ethanol can be considered orientationally relaxed during translocation.

CONCLUSION

In this contribution, we have generalized, to 2D free-energy and diffusivity landscapes, an approach that reconciles importance-sampling simulations with the determination of kinetic parameters. The novelty of this generalization lies in the explicit introduction of an angular coordinate in addition to the translational one. The method is probed in the cases of a water and an ethanol molecule permeating a model biological membrane consisting of a pure, fully hydrated POPC bilayer. The very nature of water is reflected in the 2D potential of mean force, bereft of significant orientational preference, even at the aqueous interfaces. In the case of ethanol, however, we find a free-energy minimum of −1 kcal/mol when the molecule is located between the lipid head groups and the hydrophobic core of the bilayer and oriented, so that the hydroxyl moiety strongly interacts with the head groups, while the ethyl moiety is in contact with the lipid tails. Such a configuration of the solute, with respect to the membrane, can only be obtained at the price of its complete rotation in the lipid environment, thereby warranting the explicit inclusion of an angular dependence in the free energy. The diffusive model that we have constructed demonstrates that orientational relaxation of ethanol is possible during a typical translocation event. Yet, for larger permeants, the orientational relaxation time may be comparable or longer than the time scale spanned by translocation, making consideration of the orientation indispensable.

Neglecting reorientation of the permeant is tantamount to assuming orientational average in the evaluation of the force, which may be true over sufficiently long simulation times. Barring paradigmatically small permeants, under most circumstances, this assumption is, however, not warranted. In fact, omission of the orientational degree of freedom in the importance-sampling simulation may result in nonergodicity scenarios, wherein the permeant does not have the time to reorient as it diffuses translationally across the lipid bilayer. It follows that exploration of phase space is partially amputated, which, in turn, is likely to yield inaccurate estimates of the free energy and, by ricochet, of the diffusivity. One might argue that, for small permeants endowed with fast reorientation relaxation times, this problem may not become apparent. This is probably true in the case of equilibrium importance-sampling methods, with time-dependent biases. However, the same cannot be said for nonequilibrium work methods, wherein the solute is envisioned to be dragged too fast to allow orientational degrees of freedom to be visited adequately. Even in the case of equilibrium importance-sampling simulations, the issue of frustrated exploration of transition-coordinate space is anticipated to become acute for bulky and flexible permeants. Over the time scales spanned by translocation across the lipid bilayer in these simulations, large solutes are likely to diffuse in the same orientation, resulting in an improbable alignment of the their dipole moment with the static electric field created by the mirror aqueous interface, on the other side of the bilayer. Such a misalignment bears severe consequences inasmuch as the balance between electrostatic and nonelectrostatic forces at the interface, and, hence, the underlying free energy are concerned. Therefore, attention should be paid when preparing stratified free-energy calculations, wherein the permeant is translated artificially along the reaction pathway by means of large external forces, yielding thermodynamically questionable orientations in the different windows, notably at the two aqueous interfaces of the model membrane.

In addition to its direct relevance for biology and medicine, passive translocation of permeants across lipid bilayers can be considered as a model system for many other transport processes. Because of the intrinsic lateral symmetry of pure lipid bilayers, they permit transport phenomena to be investigated without the complications induced by heterogeneous systems, and serve as a test bed for the development of methods capable of tackling more intricate molecular assemblies. Indeed, the developments described herein could prove useful for elucidating the role of orientational and conformational kinetics in permeation through membrane proteins.[25]

ASSOCIATED CONTENT

Supporting Information

One figure, showing the orientational diffusivity calculated for free ethanol, is provided as Supporting Information. This

dx.doi.org/10.1021/ct500209j | J. Chem. Theory Comput. XXXX, XXX, XXX−XXX

material is available free of charge via the Internet at http://pubs.acs.org/.

AUTHOR INFORMATION

Corresponding Author

*E-mail: chipot@ks.uiuc.edu.

Notes

The authors declare no competing financial interest.

ACKNOWLEDGMENTS

The authors acknowledge useful input from Dr. Jérôme Hénin, Institut de Biologie Physico-Chimique in Paris, for the design of the two-dimensional transition coordinate. J.C. thanks Dr. Zhaleh Ghaemi, Department of Chemistry, University of Illinois at Urbana−Champaign, for helpful discussion. They are indebted to the Centre Informatique National de l'Enseignement Supérieur in Montpellier for their generous allocation of computer time.

REFERENCES

(1) Diamond, J. M.; Katz, Y. Interpretation of Nonelectrolyte Partition Coefficients Between Dimyristoyl Lecithin and Water. *J. Membr. Biol.* **1974**, *17*, 121−154.

(2) Xiang, T.-X.; Anderson, B. The Relationship Between Permeant Size and Permeability in Lipid Bilayer Membranes. *J. Membr. Biol.* **1994**, *140*, 111−122.

(3) Adson, A.; Burton, P. S.; Raub, T. J.; Barsuhn, C. L.; Audus, K. L.; Ho, N. F. Passive Diffusion of Weak Organic Electrolytes Across Caco-2 Cell Monolayers: Uncoupling the Contributions of Hydrodynamic, Transcellular, and Paracellular Barriers. *J. Pharm. Sci.* **1995**, *84*, 1197−1204.

(4) Kansy, M.; Senner, F.; Gubernator, K. Physicochemical High Throughput Screening: Parallel Artificial Membrane Permeation Assay in the Description of Passive Absorption Processes. *J. Med. Chem.* **1998**, *41*, 1007−1010.

(5) Kansy, M.; Avdeef, A.; Fischer, H. Advances in Screening for Membrane Permeability: High-Resolution PAMPA for Medicinal Chemists. *Drug Discovery Today: Technol.* **2004**, *1*, 349−355.

(6) Avdeef, A.; Artursson, P.; Neuhoff, S.; Lazorova, L.; Gråsjö, J.; Tavelin, S. Caco-2 Permeability of Weakly Basic Drugs Predicted with the Double-Sink PAMPA Method. *Eur. J. Pharm. Sci.* **2005**, *24*, 333−349.

(7) Marrink, S.; Berendsen, H. Simulation of Water Transport through a Lipid Membrane. *J. Phys. Chem.* **1994**, *98*, 4155−4168.

(8) Bemporad, D.; Essex, J. W.; Luttmann, C. Permeation of Small Molecules through a Lipid Bilayer: A Computer Simulation Study. *J. Phys. Chem. B* **2004**, *108*, 4875−4884.

(9) Orsi, M.; Essex, J. W. In *Molecular Simulations and Biomembranes: From Biophysics to Function*; Sansom, M. P., Biggin, P. C., Eds.; RSC Publishing: Cambridge, U.K., 2010; Chapter 4, pp 76−90.

(10) Wei, C.; Pohorille, A. Permeation of Nucleosides through Lipid Bilayers. *J. Phys. Chem. B* **2011**, *115*, 3681−3688.

(11) Cardenas, A. E.; Jas, G. S.; DeLeon, K. Y.; Hegefeld, W. A.; Kuczera, K.; Elber, R. Unassisted Transport of *N*-acetyl-L-tryptophanamide through Membrane: Experiment and Simulation of Kinetics. *J. Phys. Chem. B* **2012**, *116*, 2739−2750.

(12) Holland, B. W.; Gray, C. G.; Tomberli, B. Calculating Diffusion and Permeability Coefficients with the Oscillating Forward−Reverse Method. *Phys. Rev. E* **2012**, *86*, 036707.

(13) Ghaemi, Z.; Minozzi, M.; Carloni, P.; Laio, A. A Novel Approach to the Investigation of Passive Molecular Permeation through Lipid Bilayers from Atomistic Simulations. *J. Phys. Chem. B* **2012**, *116*, 8714−8721.

(14) Swift, R. V.; Amaro, R. E. Back to the Future: Can Physical Models of Passive Membrane Permeability Help Reduce Drug Candidate Attrition and Move Us Beyond QSPR? *Chem. Biol. Drug Des.* **2013**, *81*, 61−71.

(15) Neale, C.; Madill, C.; Rauscher, S.; Pomès, R. Accelerating Convergence in Molecular Dynamics Simulations of Solutes in Lipid Membranes by Conducting a Random Walk Along the Bilayer Normal. *J. Chem. Theory Comput.* **2013**, *9*, 3686−3703.

(16) Bonhenry, D.; Tarek, M.; Dehez, F. Effects of Phospholipid Composition on the Transfer of a Small Cationic Peptide across a Model Biological Membrane. *J. Chem. Theory Comput.* **2013**, *9*, 5675−5684.

(17) Comer, J.; Schulten, K.; Chipot, C. Calculation of Lipid-Bilayer Permeabilities Using an Average Force. *J. Chem. Theory Comput.* **2014**, *10*, 554−564.

(18) Chipot, C.; Pohorille, A. In *Free Energy Calculations*; Springer: Berlin, Heidelberg, New York, 2007; pp 81−115.

(19) Lelièvre, T.; Stoltz, G.; Rousset, M. In *Free Energy Computations: A Mathematical Perspective*; World Scientific: Singapore, 2010; pp 1−60.

(20) Hummer, G. Position-Dependent Diffusion Coefficients and Free Energies from Bayesian Analysis of Equilibrium and Replica Molecular Dynamics Simulations. *New J. Phys.* **2005**, *7*, 34.

(21) Parisio, G.; Stocchero, M.; Ferrarini, A. Passive Membrane Permeability: Beyond the Standard Solubility-Diffusion Model. *J. Chem. Theory Comput.* **2013**, *9*, 5236−5246.

(22) Kopelevich, D. I. One-Dimensional Potential of Mean Force Underestimates Activation Barrier for Transport across Flexible Lipid Membranes. *J. Chem. Phys.* **2013**, *139*, 134906.

(23) Bemporad, D.; Luttmann, C.; Essex, J. Behaviour of Small Solutes and Large Drugs in a Lipid Bilayer from Computer Simulations. *Biochim. Biophys. Acta Biomembr.* **2005**, *1718*, 1−21.

(24) Hamming, R. W. *Numerical Methods for Scientists and Engineers*; McGraw−Hill: New York, 1962; pp 3−4.

(25) Hénin, J.; Tajkhorshid, E.; Schulten, K.; Chipot, C. Diffusion of Glycerol through *Escherichia Coli* Aquaglyceroporin GlpF. *Biophys. J.* **2008**, *94*, 832−839.

(26) Türkcan, S.; Alexandrou, A.; Masson, J. A Bayesian Inference Scheme to Extract Diffusivity and Potential Fields from Confined Single-Molecule Trajectories. *Biophys. J.* **2012**, *102*, 2288−2298.

(27) Comer, J. R.; Chipot, C. J.; Gonzalez-Nilo, F. D. Calculating Position-Dependent Diffusivity in Biased Molecular Dynamics Simulations. *J. Chem. Theory Comput.* **2013**, *9*, 876−882.

(28) Darve, E.; Pohorille, A. Calculating Free Energies Using Average Force. *J. Chem. Phys.* **2001**, *115*, 9169−9183.

(29) Hénin, J.; Chipot, C. Overcoming Free Energy Barriers Using Unconstrained Molecular Dynamics Simulations. *J. Chem. Phys.* **2004**, *121*, 2904−2914.

(30) Micheletti, C.; Bussi, G.; Laio, A. Optimal Langevin Modeling of Out-of-equilibrium Molecular Dynamics Simulations. *J. Chem. Phys.* **2008**, *129*, 074105.

(31) Ljubetič, A.; Urbančič, I.; Štrancar, J. Recovering Position-Dependent Diffusion from Biased Molecular Dynamics Simulations. *J. Chem. Phys.* **2014**, *140*, 084109.

(32) Comer, J.; Dehez, F.; Cai, W.; Chipot, C. Water Conduction Through a Peptide Nanotube. *J. Phys. Chem. C* **2013**, *117*, 26797−26803.

(33) von Toussaint, U. Bayesian Inference in Surface Physics. *Rev. Mod. Phys.* **2011**, *83*, 943−999.

(34) Dose, V. Bayesian Inference in Physics: Case Studies. *Rep. Prog. Phys.* **2003**, *66*, 1421.

(35) Best, R.; Hummer, G. Diffusion Models of Protein Folding. *Phys. Chem. Chem. Phys.* **2011**, *13*, 16902−16911.

(36) Metropolis, N.; Rosenbluth, M.; Rosenbluth, A.; Teller, A.; Teller, E. Equation of State Calculations by Fast Computing Machines. *J. Chem. Phys.* **1953**, *21*, 1087−1092.

(37) Ermak, D.; McCammon, J. Brownian Dynamics with Hydrodynamic Interactions. *J. Chem. Phys.* **1978**, *69*, 1352.

(38) Noskov, S. Y.; Im, W.; Roux, B. Ion Permeation through the α-Hemolysin Channel: Theoretical Studies Based on Brownian Dynamics and Poisson−Nernst−Plank Electrodiffusion Theory. *Biophys. J.* **2004**, *87*, 2299−2309.

(39) Hénin, J.; Fiorin, G.; Chipot, C.; Klein, M. Exploring Multidimensional Free Energy Landscapes Using Time-Dependent Biases on Collective Variables. *J. Chem. Theory Comput.* **2009**, *6*, 35−47.
(40) Schulten, K. Non-Equilibrium Statistical Mechanics: Lecture Notes, 1999; http://www.ks.uiuc.edu/Services/Class/PHYS498/LectureNotes.html (accessed May 7, 2014).
(41) Phillips, J. C.; Braun, R.; Wang, W.; Gumbart, J.; Tajkhorshid, E.; Villa, E.; Chipot, C.; Skeel, R. D.; Kale, L.; Schulten, K. Scalable Molecular Dynamics with NAMD. *J. Comput. Chem.* **2005**, *26*, 1781−1802.
(42) Feller, S. E.; Zhang, Y. H.; Pastor, R. W.; Brooks, B. R. Constant Pressure Molecular Dynamics Simulations—The Langevin Piston Method. *J. Chem. Phys.* **1995**, *103*, 4613−4621.
(43) Darden, T. A.; York, D. M.; Pedersen, L. G. Particle Mesh Ewald: An *N* log *N* Method for Ewald Sums in Large Systems. *J. Chem. Phys.* **1993**, *98*, 10089−10092.
(44) Klauda, J.; Venable, R.; Freites, J.; O'Connor, J.; Tobias, D.; Mondragon-Ramirez, C.; Vorobyov, I.; MacKerell, A., Jr.; Pastor, R. Update of the CHARMM All-Atom Additive Force Field for Lipids: Validation on Six Lipid Types. *J. Phys. Chem. B* **2010**, *114*, 7830−7843.
(45) Vanommeslaeghe, K.; Hatcher, E.; Acharya, C.; Kundu, S.; Zhong, S.; Shim, J.; Darian, E.; Guvench, O.; Lopes, P.; Vorobyov, I.; MacKerell, A. D. CHARMM General Force Field: A Force Field for Drug-like Molecules Compatible with the CHARMM All-atom Additive Biological Force Fields. *J. Comput. Chem.* **2010**, *31*, 671−690.
(46) Tuckerman, M. E.; Berne, B. J.; Martyna, G. J. Reversible Multiple Time Scale Molecular Dynamics. *J. Phys. Chem. B* **1992**, *97*, 1990−2001.
(47) Miyamoto, S.; Kollman, P. A. SETTLE: An Analytical Version of the SHAKE and RATTLE Algorithm for Rigid Water Molecules. *J. Comput. Chem.* **1992**, *13*, 952−962.
(48) Andersen, H. Rattle: A "Velocity" Version of the Shake Algorithm for Molecular Dynamics Calculations. *J. Comput. Phys.* **1983**, *52*, 24−34.
(49) Fiorin, G.; Klein, M. L.; Hénin, J. Using Collective Variables to Drive Molecular Dynamics Simulations. *Mol. Phys.* **2013**, *111*, 3345−3362.
(50) Ben-Naim, A.; Marcus, Y. Solvation Thermodynamics of Nonionic Solutes. *J. Chem. Phys.* **1984**, *81*, 2016.
(51) Berger, O.; Edholm, O.; Jähnig, F. Molecular Dynamics Simulations of a Fluid Bilayer of Dipalmitoylphosphatidylcholine at Full Hydration, Constant Pressure, and Constant Temperature. *Biophys. J.* **1997**, *72*, 2002−2013.
(52) Berendsen, H. J. C.; Postma, J. P. M.; van Gunsteren, W. F.; Hermans, J. In *Intermolecular Forces: Proceedings of the Fourteenth Jerusalem Symposium on Quantum Chemistry and Biochemistry*; Pullman, B., Ed.; D. Reidel Publishing Company: Hingham, MA, 1981; pp 331−342.
(53) Neria, E.; Fischer, S.; Karplus, M. Simulation of Activation Free Energies in Molecular Systems. *J. Chem. Phys.* **1996**, *105*, 1902.
(54) Horn, H. W.; Swope, W. C.; Pitera, J. W.; Madura, J. D.; Dick, T. J.; Hura, G. L.; Head-Gordon, T. Development of an Improved Four-Site Water Model for Biomolecular Simulations: TIP4P-Ew. *J. Chem. Phys.* **2004**, *120*, 9665.
(55) Wang, J.; Wolf, R. M.; Caldwell, J. W.; Kollman, P. A.; Case, D. A. Development and Testing of a General Amber Force Field. *J. Comput. Chem.* **2004**, *25*, 1157−1174.
(56) Jójárt, B.; Martinek, T. A. Performance of the General Amber Force Field in Modeling Aqueous POPC Membrane Bilayers. *J. Comput. Chem.* **2007**, *28*, 2051−2058.